$Al_2O_3/NbAlO/Al_2O_3$ sandwich gate dielectric film on InP

Xinhong Cheng, Dapeng Xu, Qing-Qing Sun, Dawei He, Zhongjian Wang, Yuehui Yu, David Wei Zhang, and Qingtai Zhao

Citation: Appl. Phys. Lett. **96**, 022904 (2010);
View online: https://doi.org/10.1063/1.3292217
View Table of Contents: http://aip.scitation.org/toc/apl/96/2
Published by the American Institute of Physics

$Al_2O_3/NbAlO/Al_2O_3$ sandwich gate dielectric film on InP

Xinhong Cheng,[1,a)] Dapeng Xu,[1] Qing-Qing Sun,[2] Dawei He,[1] Zhongjian Wang,[1] Yuehui Yu,[1] David Wei Zhang,[2] and Qingtai Zhao[3]
[1]*State Key Laboratory of Functional Materials for Informatics, SIMIT, Chinese Academy of Sciences, Changning Road 865, Shanghai 200050, People's Republic of China*
[2]*State Key Laboratory of ASIC and System, School of Microelectronics, Fudan University, Shanghai 200433, People's Republic of China*
[3]*Forschungszentrum Jülich GmbH, Jülich 52425, Germany*

(Received 24 November 2009; accepted 21 December 2009; published online 13 January 2010)

$Al_2O_3/NbAlO/Al_2O_3$ sandwich dielectric films were grown on InP substrate and annealed. X-ray reflectivity measurements suggested that 1.0 nm interfacial layer existed at InP interface, x-ray diffraction and high resolution transmission electron microscopy indicated the films were crystallized. X-ray photoelectron spectra indicated the oxidization of InP substrate, and the valence-band offset between the dielectric film and InP interface was calculated to be 3.1 eV. The electrical measurements indicated that the leakage current density was 40 mA/cm^2 at gate bias of 1 V, and the equivalent oxide thickness and the dielectric constant were 1.7 and 20 nm, respectively. © *2010 American Institute of Physics*. [doi:10.1063/1.3292217]

The future scaling of complementary metal-oxide semiconductor (CMOS) according to Moore's law will meet fundamental physical limit, several advanced technologies such as high *k* gate dielectrics, metal gates, and high mobility channels have been widely demanded. With tremendous efforts to the development of high *k* gate dielectrics, the application of high mobility III–V compound channels for CMOS have presented exciting device performance.[1–3] Passlack group have fabricated GaAs-based *n*-type device with the use of GdGaO gate dielectric stacks, where the interface state density and leakage current was only $2\times10^{11}/(cm^2\,eV)$ and $10^{-9}-10^{-8}$ A/cm^2, respectively, and the electron mobility exceeded 6000 $cm^2/(V\,s)$. Ye group prepared GaAs NMOSFET with Al_2O_3 gate dielectrics, where the maximum drain current was 1.05 A/mm, and the transconductance reached to 350 mS/mm. Ye group also gave some results on InP-based MOSFET with HfO_2 or Al_2O_3 gate dielectrics,[4] where the gate leakage current less than 10 $\mu A/mm$, the peak effective mobility is 650 $cm^2/V\,s$. The hump and stretch-out in C–V curves for InP-based capacitors was very serious, due to Fermi level pinning originated from unstable and defect-rich gate stacks.[5] Furthermore, the data about high *k* on InP was relatively small, it is necessary to further study the performance of high *k* dielectrics on InP. Al_2O_3 has widely used as blocking layer or capping oxide layer due to its wide gap and good thermal stability and easy introduction interface dipoles.[6] Nb_2O_5 with a high permittivity of 50 was usually used in memory application.[7] Kukli group[8] have mixed Nb_2O_5 into ZrO_2 or Al_2O_3 dielectrics to increase the dielectric constant, and the mixtures demonstrated hysteresis-free C–V curves with clear accumulation and quite a low dissipation in the accumulation region. According to the Ref. 9, conduction band offsets for Al_2O_3 on InP substrate was 2.9 eV, so $Al_2O_3/NbAlO/Al_2O_3$ sandwich gate dielectric structure cannot only improve the thermal stability, but also suppress the leakage effectively. Therefore, in this work, $Al_2O_3/NbAlO/Al_2O_3$ sandwich gate dielectric films were prepared by atom layer deposition (ALD) method, the microstructures and the electrical performance was analyzed.

n-type InP (100) wafer doped with sulfur ($\sim1\times10^{18}$ cm^{-3}) was cleaned by diluted-hydrofluoric before the film deposition. The flow-type ALD Reactor (F-120, ASM-Microchemistry Ltd.) was used to prepare NbAlO dielectric films. $Al(CH_3)_3$ and $Nb(OET)_5$ were metal precursors, and H_2O served as oxidant. The growth temperature was 300 °C. First, 12 cycles Al_2O_3 was grown. Second, 20 or 60 cycles $Nb_2O_5-Al_2O_3$ nanolaminates were deposited; one nanolaminates cycle was composed of eight subcycles Nb_2O_5 and one subcycle Al_2O_3. Third, 12 cycles Al_2O_3 was grown. The growth rate of one cycle was 0.3 Å and 1.2 Å for Nb_2O_5 and Al_2O_3, respectively. 12 cycles Al_2O_3/20 cycles $Nb_2O_5-Al_2O_3$ nanolaminates/12 cycles Al_2O_3 film was signed as S1. 12 cycles Al_2O_3/60 cycles $Nb_2O_5-Al_2O_3$ nanolaminates/12 cycles Al_2O_3 film was signed as S2. Then samples were cut into several parts, and some were treated in N_2 at 500 °C for 1 min. Metal-insulator-semiconductor (MIS) capacitors were formed with Pt or TiN top electrodes through a shadow mask sputtering, and bottom electrode through a blanket sputtering of Pt. Post deposition annealing in N_2 at 450 °C was performed to form ohmic contact.

X-ray reflectivity (XRR) and x-ray diffraction (XRD) measurements were carried out in Shanghai Synchrotron Radiation Facility. X-ray wavelength is 0.124 nm. In order to realize 'true specular reflectivity for rough surface,[10] XRR were measured in θ-2θ mirror reflection and longitudinal scan diffuse scattering mode, respectively, with the offset of 0.1°. The specular reflectivity was obtained by the subtraction of the diffuse scattering data from the mirror reflection data. The measured and simulated XRR data for S1 were shown in Fig. 1. Kiessig fringes in the reflectivity curve were clearly observed, which shows the presence of basic layered structure. The layer thickness can be evaluated by the width of fringe (thickness=$\lambda/2\delta\theta$, $2\delta\theta$ is the width of fringe). The width of fringe was 0.9°, and the film thickness was estimated to 8nm. Moreover, simulation model were shown in inset of Fig. 1. First, 0.9 nm low density interfacial layer

a)Electronic mail: xh_cheng@mail.sim.ac.cn.

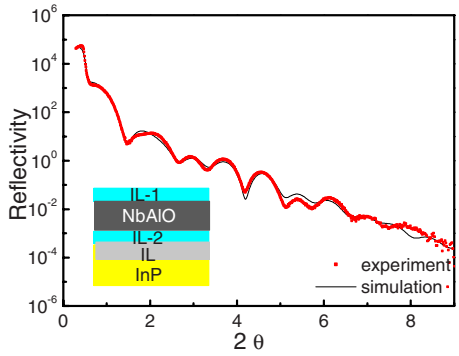

FIG. 1. (Color online) XRR data for 8.5 nm $Al_2O_3/NbAlO/Al_2O_3$ (solid line for measured, and dashed line for simulation).

(IL-1) with a roughness of 0.3 nm existed, which was corresponding to the deposition of 12 cycles Al_2O_3. Second, 4.5 nm high density NbAlO layer with the roughness of 0.9nm followed IL-1 layer, which was corresponding to 20 cycles $Nb_2O_5-Al_2O_3$ nanolaminates. Third, there was a low density IL layer (IL-2) with a thickness of 2.3 nm and a roughness of 0.4, which was analog to IL-1, coming from 12 cycles Al_2O_3. At last, there was 1.0 nm IL with the roughness of 0.5 nm at InP interface. XRR analysis showed that total film thickness of S1 was around 8.5 nm. The film thickness of S2 was around 26 nm.

XRD was employed to analyze crystal structure of S1 in in-plane grazing incidence diffraction mode and ω-2θ scan, respectively. For in-plane mode, x-ray incidence angle was fixed at 2°, and 2θ scans from 10° to 60°. Because the beam is incident at a grazing angle, the penetration depth of the beam is limited to within about 100 nm of the surface, the in-plane diffraction measured lattice planes nearly perpendicular to the sample surface and is mainly used in the thin film phase analysis.[11] ω-2θ diffraction measured lattice planes parallel to the sample surface. As shown in Fig. 2(a), there was one diffraction peak at 2θ=41.5°, indicating that vertical lattice planes existed and $Al_2O_3/NbAlO/Al_2O_3$ film was crystallized. There were two peaks in Fig. 2(b), locating at 2θ of 24.3° and 50°, which originated from InP substrate (200) and (400) crystal plane, respectively. In-plane XRD measurement indicated that $Al_2O_3/NbAlO/Al_2O_3$ film was crystallized after 500 °C annealing treatment.

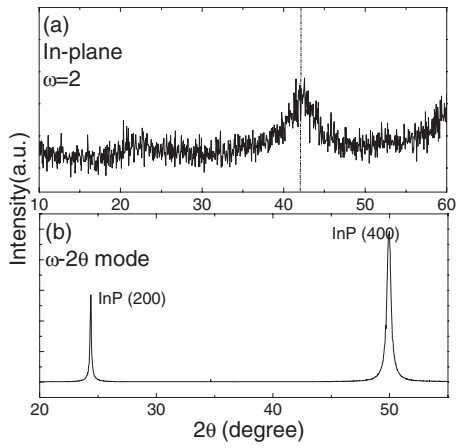

FIG. 2. XRD data for 8.5 nm $Al_2O_3/NbAlO/Al_2O_3$: (a) in-plane grazing incident diffraction mode and (b) ω-2θ scan mode.

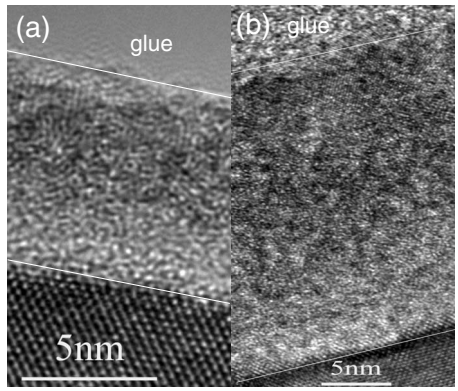

FIG. 3. HRTEM images: (a) 8.5 nm $Al_2O_3/NbAlO/Al_2O_3$ and (b) 27 nm $Al_2O_3/NbAlO/Al_2O_3$.

CM200FEG instrument was used for high resolution transmission electron microscopy (HRTEM). Figure 3 showed the dielectric films were crystallized, and the crystal structure was significant for the thick dielectric film. Laminate structure of the dielectric films could not be distinguished clearly, and the thickness for S1 and S2 was 8.5 and 27 nm, respectively. The results from HRTEM were consistent with XRR and XRD.

XPS measurements were performed to determine the chemical structure of $Al_2O_3/NbAlO/Al_2O_3$ film with Axis Ultra DLD equipment and use of Al Kα. The binding energy was calibrated with the position of C 1*s* peak at 284.8 eV.

As shown in Fig. 4, P 2*p* peak coming from InP substrate located at 129.1 eV. A peak appeared at 134.5 eV for S1, which originated from the oxidized state of P atoms.[12] This indicated the oxidization of InP substrate took place, which was consistent with XRR analysis. Al 2*p* peak located at 74.1 eV for S1 but it shifted down to 73.9eV for S2. Nb 3*d* spectrum exhibited two peaks at 207.2 and 209.8 eV for S1, and they shifted somewhat up for S2. Pauling's electronegativity of Al and Nb was 1.61 and 1.6 eV, respectively. Electrons of Nb atoms were relatively easy to transfer to Al–O bonds in Nb aluminates, resulting in a down-shift of Al 2*p* core level in NbAlO relative to pure Al_2O_3 and upshift of Nb 3*d* core level in NbAlO relative to pure Nb_2O_5. Analytical depth of x-ray was about 9 nm, and only upper part of S2 could be reached by x-ray. Therefore, Al 2*p* in-

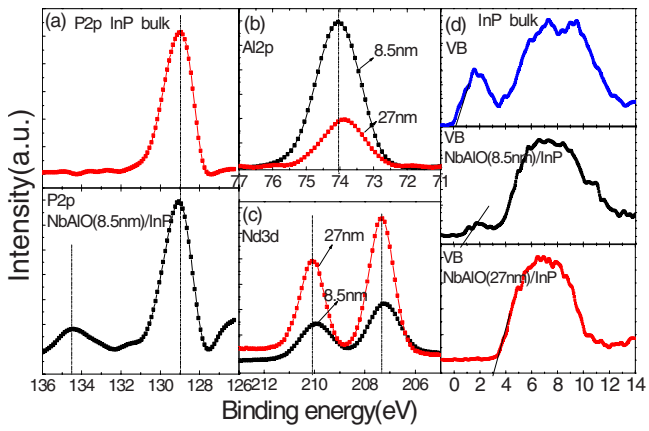

FIG. 4. (Color online) XPS spectra: (a) P 2*p*, (b) Al 2*p*, (c) Nb 3*d*, and (d) valence band spectra.

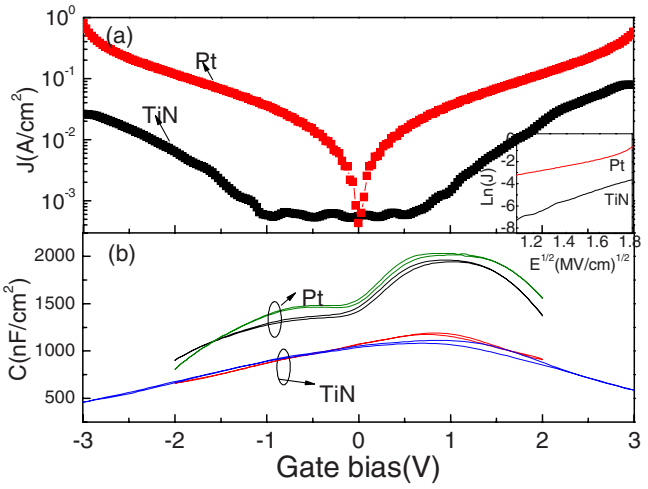

FIG. 5. (Color online) (a) Leakage current characteristics, the inset is the plots of ln(J) vs $E^{1/2}$ and (b) capacitance characteristics of MIS capacitors made of 8.5 nm dielectric film.

tensity was higher and Nb 3*d* intensity was lower in S1 than that in S2. The valence-band (VB) spectra were shown in Fig. 4(d). The VB edge of n-InP substrate was determined to be 0.1 eV by the linear extrapolation method. For S1, VB edge was 0.3 eV, and the VB edge was 3eV for S2. According to the method of Kraut, etc.,[13] the VB offset value between the dielectric film and InP can be calculated by:

$$\triangle E_V = (E_{CL}^{P\ 2p} - E_V^{InP})_{InP} - (E_{CL}^{Al\ 2p} - E_V^{NbAlO})_{thick\ NbAlO} + (E_{CL}^{Al\ 2p} - E_{CL}^{P\ 2p})_{NbAlO/InP}, \quad (1)$$

where $E_{CL}^{Al\ 2p}$ and $E_{CL}^{P\ 2p}$ were Al 2*p* and P 2*p* core levels, and E_V^{InP} and E_V^{NbAlO} were VB edge for InP substrate and S2 sample. VBO between the dielectric film and InP interface was calculated to be 3.1 eV, which was low compared to the reported calculated value by Robertson[9] (VBO between Al_2O_3 and InP was 4.5 eV). This was due to that Nb_2O_5 in the dielectric film decrease the energy gap, and the gap of the dielectric film was not high as pure Al_2O_3.

The leakage current (J–V) and the capacitance (C–V) of MIS capacitors were characterized by Agilent 4156C and Agilent 4294 Precision LCR meter at 500 kHz and 1 MHz. According to the theory of Yang,[14] the actual frequency independent capacitance was obtained from the measured capacitance at two different measuring frequencies. Here the thickness of the dielectric film was 8.5nm characterized by HRTEM.

As shown in Fig. 5(a), J–V curve was symmetrical for the MIS capacitors with Pt electrode, and leakage current increased quickly to 600 mA/cm^2 when the gate bias increased to 3 V. However, J–V curve showed an asymmetry between forward and reverse bias for that with TiN electrode, and the leakage current kept at 1 mA/cm^2 until the gate bias was higher than 1.5 V, and then it increased to 25 mA/cm^2 at the gate bias of 3 V. The inset illustrated the logarithmic current densities ln(J) as a function of the square root of electric field $E^{1/2}$ at room temperature. A fair linear tendency of the plot for ln(J) versus $E^{1/2}$ at higher electrical field (1.1–1.8 MV/cm) was achieved, indicating that Schottky emission mechanism dominated the leakage and Schottky barrier height was higher for TiN electrode than Pt.[15]

Figure 5(b) showed C–V curves of MIS capacitors with Pt and TiN electrode. Frequency dispersion between 500 kHz and 1 MHz were obtained. The capacitors with Pt electrode showed normal high frequency C–V characteristics but the capacitance in accumulation region and inversion region decreased rapidly. This was due to serious leakage for Pt electrode. Capacitors with TiN electrode showed poor C–V characteristics, implying severe Fermi level pinning. The accumulation capacitance was 2033 nF/cm^2, and the equivalent oxide thickness and the dielectric constant were estimated to 1.7 and 20 nm, respectively.

In conclusion, $Al_2O_3/NbAlO/Al_2O_3$ sandwich structures were formed by ALD. The existence of Al_2O_3 improved VBO of NbAlO film to 3.1 eV, MIS capacitors with Pt metal gate showed good C–V characteristics with a dielectric constant of 20, and Fermi level pinning was suppressed. However, the film was crystallized, the oxidization of InP interface took place, and the leakage was high. In order to improve the electrical performance of $Al_2O_3/NbAlO/Al_2O_3$ sandwich structure, the atom ratio of Nb to Al should be further optimized, and the affect of metal gate electrode on Fermi level pinning should be further studied.

This work was supported by the following Chinese foundation: NSF (Grant No. 10775166), Zhejiang Province STF (Grant No. 2008C31002), and Wenzou STF (Grant No. G20060099).

[1]M. Passlack, R. Droopad, P. Fejes, and L. Wang, IEEE Electron Device Lett. **30**, 2 (2009).
[2]M. Passlack, R. Droopad, K. Rajagopalan, J. Abrokwah, R. Gregory, and D. Nguyen, IEEE Electron Device Lett. **26**, 713 (2005).
[3]Y. Xuan, Y. Q. Wu, and P. D. Ye, IEEE Electron Device Lett. **29**, 294 (2008).
[4]Y. Q. Wu, Y. Xuan, T. Shen, P. D. Ye, Z. Cheng, and A. Lochtefeld, Appl. Phys. Lett. **91**, 022108 (2007).
[5]J. Robertson, O. Sharia, and A. A. Demkov, Appl. Phys. Lett. **91**, 132912 (2007).
[6]L. Lin and J. Robertson, Appl. Phys. Lett. **95**, 012906 (2009).
[7]J. A. Kittl, K. Opsomer, M. Popovici, N. Menou, B. Kaczer, X. P. Wang, C. Adelmann, M. A. Pawlak, K. Tomida, A. Rothschild, B. Govoreanu, R. Degraeve, M. Schaekers, M. Zahid, A. Delabie, J. Meersschaut, W. Polspoel, S. Clima, G. Pourtois, W. Knaepen, C. Detavernier, V. V. Afanas'ev, T. Blomberg, D. Pierreux, J. Swerts, P. Fischer, J. W. Maes, D. Manger, W. Vandervorst, T. Conard, A. Franquet, P. Favia, H. Bender, B. Brijs, S. Van Elshocht, M. Jurczak, J. Van Houdt, and D. J. Wouters, Microelectron. Eng. **86**, 1789 (2009).
[8]K. Kukli, M. Ritala, M. Leskel€a, T. Sajavaara, J. Keinonen, D. Gilmer, S. Bagchi, and L. Prabhu, J. Non-Cryst. Solids **303**, 35 (2002).
[9]J. Robertson and B. Falabretti, J. Appl. Phys. **100**, 014111 (2006).
[10]A. Gibaud and S. Hazra, Curr. Sci. **78**, 1467 (2000).
[11]S. Takahashi, M. Taniguchi, K. Omote, N. Wakabayashi, R. Tanaka, and A. Yamagishi, Chem. Phys. Lett. **352**, 213 (2002).
[12]C. Robert-Goumet, G. Monier, B. Zefack, S. Chelda, L. Bideux, B. Gruzza, and O. K. Awitor, Surf. Sci. **603**, 2923 (2009).
[13]E. Kraut, R. Grant, J. Waldrop, and K. Kowalczyk, Phys. Rev. B **28**, 1965 (1983).
[14]K. J. Yang and C. Hu, IEEE Trans. Electron Devices **46**, 1500 (1999).
[15]L. Shi, Y. D. Xia, B. Xu, J. Yin, and Z. G. Liu, J. Appl. Phys. **101**, 034102 (2007).